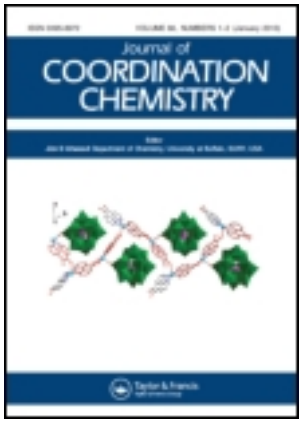

Journal of Coordination Chemistry
Publication details, including instructions for authors and subscription information:
http://www.tandfonline.com/loi/gcoo20

Self-assembly of a 3-D self-catenated framework based on $[V_4O_{12}]^{4-}$ polyoxoanions and cobalt-organic polymer

Yan-Fei Qi [a], Kun Xu [a], Li-Jun Lu [b], Juan Li [a] & En-Bo Wang [c]
[a] School of Public Health, Jilin University, Changchun, China
[b] JiLin Entry-Exit Inspection and Quarantine Bureau, Changchun, China
[c] Key Laboratory of Polyoxometalates Science of Ministry of Education, Department of Chemistry, Northeast Normal University, Changchun, China
Accepted author version posted online: 21 Feb 2013.Published online: 05 Apr 2013.

To cite this article: Yan-Fei Qi, Kun Xu, Li-Jun Lu, Juan Li & En-Bo Wang (2013) Self-assembly of a 3-D self-catenated framework based on $[V_4O_{12}]^{4-}$ polyoxoanions and cobalt-organic polymer, Journal of Coordination Chemistry, 66:7, 1228-1237, DOI: 10.1080/00958972.2013.777835

To link to this article: http://dx.doi.org/10.1080/00958972.2013.777835

Journal of Coordination Chemistry, 2013
http://dx.doi.org/10.1080/00958972.2013.777835

Self-assembly of a 3-D self-catenated framework based on $[V_4O_{12}]^{4-}$ polyoxoanions and cobalt-organic polymer

YAN-FEI QI*†, KUN XU†, LI-JUN LU‡, JUAN LI*† and EN-BO WANG§

†School of Public Health, Jilin University, Changchun, China
‡JiLin Entry-Exit Inspection and Quarantine Bureau, Changchun, China
§Key Laboratory of Polyoxometalates Science of Ministry of Education, Department of Chemistry, Northeast Normal University, Changchun, China

(*Received 15 November 2012; in final form 30 January 2013*)

Reaction of a flexible ligand with cobalt salt in the presence of polyoxovanadate produces a new composite solid, $Co_2(btx)_4V_4O_{12}$, **1** (btx = 1,4-bis(triazol-1-ylmethyl)benzene). The structure of **1** was determined by single-crystal X-ray diffraction analysis and further characterized by elemental analysis, IR spectrum, and TG analysis. Compound **1** exhibits a 3-D 4,6-connected self-catenated net constructed from $[V_4O_{12}]^{4-}$ building blocks and the $\{Co(btx)_2\}^{2+}$ 3-D metal-organic cation polymer. The electronic properties of **1** have been investigated.

Keywords: Polyoxovanadates; Entangled networks; Organic–inorganic hybrid; Electrochemical property

1. Introduction

Entangled systems, one of the major themes of supramolecular chemistry, are common in biology, as seen in catenanes, rotaxanes, and molecular knots, and have attracted considerable attention because of their properties, complicated architectures, and topologies [1–4]. A variety of interpenetrated nets, in which only internal connections are broken to separate individual nets, have been reported and reviewed [5, 6]. Most of the entangled structures exist in metal-organic frameworks (MOFs) with different dimensions. However, little research has been performed with polyoxometalate (POM)-based entangled structures [7–11]. Polyoxovanadate is a subclass of the family of POMs, which shows a great diversity in its structure [12–14]. The structural variety is derived from its multiple oxidation states (III, IV, and V) and coordination geometries (tetrahedral, square pyramidal, and octahedral). These features make it much easier to control the size, shape, and charge distribution at the molecular level. Flexibility in the structure makes it possible to fine-tune the redox potentials, acidities, and reactivities of polyoxovanadate, endowing these solid materials with intriguing topologies and fascinating properties [15–18]. Others [19] and we [20, 21] demonstrated in recent contributions that such polyanions with metal-organic

*Corresponding authors. Email: qiyanfei@jlu.edu.cn (Y.-F. Qi); Li_juan@jlu.edu.cn (J. Li)

polymers produce a series of hybrid materials, including some interesting entangled structures. In these extended hybrids, the polyoxovanadates play several important roles. They can function as nonbonding guests or anion templates to control the structure-forming processes [22]. Moreover, they can behave as versatile connectors and linkers to take part in the whole structure, such as $[H_4V_{18}O_{46}(SiO)_8(DAB)_4{\cdot}(H_2O)]{\cdot}4H_2O$ [23].

Judicious selection of ligands in constructing entangled frameworks is very important because changes about organic building blocks, such as length, flexibility, and symmetry, can dramatically change the final structural motifs of these coordination frameworks. Although many factors can influence the formation of networks with interpenetrating character, such as the bulkiness of the ligands and of the counter-ions, the presence of π–π interactions between aromatic bridging ligands, coordination, etc. [24], it can be said that the larger the voids in a net, the more likely interpenetration is to occur and the greater the number of independent nets a particular void is passed through. In general, longer ligands will lead to larger voids. Recent studies on crystal engineering of 3-D frameworks suggest that linear flexible N,N′-bridging ligands, such as 1,4-bis(triazol-1-ylmethyl)benzene, connect metal ions forming networks with interpenetrating character [25]. The transition metal/biim complex and polyoxovanadates have been chosen to form 3-D networks. Herein, we report a new 3-D 4,6-connected self-catenated compound, $Co_2(btx)_4V_4O_{12}$, **1** (btx = 1,4-bis(triazol-1-ylmethyl)benzene). The electrochemistry of **1** has also been studied.

2. Experimental

2.1. *Materials and methods*

All chemicals were commercially purchased and used without purification. Elemental analyzes (C, H, and N) were performed on a Perkin-Elmer 2400 CHN Elemental Analyzer. Vanadium was determined by a Leaman inductively coupled plasma spectrometer. IR spectra were recorded from 400–4000 cm^{-1} on an Alpha Centaurt FT/IR Spectrophotometer using KBr pellets. TG analyzes were performed on a Perkin-Elmer TGA7 instrument in flowing N_2 with a heating rate of 10 °C min^{-1}. A CHI 660 electrochemical workstation connected to a Digital-586 personal computer was used for control of the electrochemical measurements and for data collection. A conventional three-electrode system was used. The working electrode was compound **1** bulk-modified carbon paste electrodes (CPEs). A saturated calomel electrode was used as reference electrode and Pt gauze as a counter electrode. The working electrodes were prepared following our earlier method [26].

2.2. *Synthesis of $Co_2(btx)_4V_4O_{12}$ (1)*

A mixture of $NaVO_3$ (0.3 mmol), $CoCl_2{\cdot}6H_2O$ (0.3 mmol), btx (0.5 mmol) and NaH_2PO_4 (0.1 mmol) was dissolved in deionized water (6 mL) and stirred for 30 min in air. Then, the solution was sealed in a 15 mL Teflon-lined bomb at 120 °C for 5 days. After slowly cooling the bomb to room temperature, the resulting orange crystals of **1** were collected from the mother liquid (yield: ca. 59% based on V). The crystals were washed with distilled water and dried at ambient temperature. Anal. Calcd $C_{24}H_{28}CoN_{12}O_6V_2$ (**1**) (%): C, 38.88; H, 3.81; N, 22.67; Co, 7.95; V, 13.74. Found (%): C, 39.01; H, 3.89; N, 22.62; Co, 7.91;

Table 1. Crystal data and structure refinement for **1**.

	1
Formula	$C_{24}H_{28}CoN_{12}O_6V_2$
M_r	741.39
T (K)	296(2)
Crystal system	Tetragonal
Space group	$I4(1)/a$
a (Å)	16.3374(1)
b (Å)	16.3374(1)
c (Å)	26.461(4)
α (°)	90
β (°)	90
γ (°)	90
V (Å^3)	7062.7(1)
Z	8
ρ_{Calcd} (g cm^{-3})	1.395
μ (mm^{-1})	1.035
R_{int}	0.0639
Data/parameters	3076/205
Goodness of fit	1.036
$R_1{}^a$ [$I>2\sigma(I)$]	0.0637
$wR_2{}^b$ [$I>2\sigma(I)$]	0.1726
Largest residuals (e Å^{-3})	0.695/−0.515

[a] $R_1 = \sum ||F_0|-|F_c|| / \sum |F_0|$.
[b] $wR_2 = \sum[w(F_0^2 - F_c^2)_2] / \sum[w(F_0^2)_2]^{1/2}$.

Table 2. Important bond lengths [å] for **1**.

V(1)–O(1)	1.613(4)	V(1)–O(2)#1	1.776(4)
V(1)–O(3)	1.641(3)	V(1)–O(2)	1.802(4)
Co(1)–O(3)#2	2.031(3)	Co(1)–N(1)#2	2.158(4)
Co(1)–O(3)	2.031(3)	Co(1)–N(1)	2.158(4)
Co(1)–N(4)	2.168(5)	Co(1)–N(4)#2	2.168(5)

Symmetry transformations used to generate equivalent atoms: #1 $-y+3/4$, $x+3/4$, $-z-1/4$; #2 $-x$, $-y+1$,$-z$; #3 $y-3/4$, $-x+3/4$, $-z-1/4$; #4 $y+1/4$, $-x+1/4$, $z+1/4$; #5 $-y+1/4$, $x-1/4$, $z-1/4$.

V, 13.65%. IR spectrum (cm^{-1}): 3389w, 3115s, 2938w, 1794w, 1641w, 1521s, 1423s, 1351s, 1285s, 1198m, 1133s, 1012s, 954s, 908s, 811s, 730s, 642s, 513w, 465w.

2.3. *X-ray crystallography*

The structure of **1** was determined on a Bruker SMART CCD diffractometer, collected at 293 K and graphite-monochromated Mo-Kα radiation ($\lambda = 0.71073$ Å). Empirical absorption corrections were applied for **1** utilizing SADABS. The structure was solved by the direct method and refined by full-matrix least squares on F^2 using SHELXL-97 [27, 28]. Hydrogens of organic ligands were fixed in ideal positions. All nonhydrogen atoms were refined anisotropically.

A summary of crystal data and structure refinement for **1** are provided in table 1. Selected bond lengths and angles are listed in table 2. CCDC 669339 contains the supplmentary crystallographic data for this study. These data can be obtained free of charge from the Cambridge Crystallographic Data Center via www.ccdc.cam.ac.uk/data_request/cif.

3. Results and discussion

3.1. *Structure description*

The structure of $Co_2(btx)_4V_4O_{12}$ (**1**) is a unique 4,6-connected 3-D self-catenated network. The structure may be described as Co^{2+} linked by flexible btx to achieve 3-D metal-organic cationic polymers $\{Co(btx)_2\}^{2+}$; isolated $[V_4O_{12}]^{4-}$ clusters combine with the transition metal to form a 3-D bimetallic rigid inorganic framework. In the asymmetric unit of **1**, there is half Co^{II}, one V^V, one btx, and three oxygens. The eight-member anionic $[V_4O_{12}]^{4-}$ metallocycle in **1** consists of four corner sharing $\{VO_4\}$ tetrahedral units with V–O bond lengths of 1.614(4)–1.803(4) Å and O–V–O angles 106.4(2)°–111.6(2)°. All vanadium sites employ two oxo-groups in the eight-member ring and one oxo with each of the four cobalt layers; the fourth is a terminal oxo. Bond valence sum calculations give 5.30 for V. Each $[V_4O_{12}]^{4-}$, acting as a four-connected node, is linked to four others through four bridging $[CoO_2N_4]$ octahedra (O(3) and its equivalent atoms) to generate an extended neutral 3-D inorganic bimetal framework, shown in figure 1(a) and (b). The topology of inorganic bimetal frame can be described as a α-Po net that possesses open channels of approximately 19.844(7) × 14.099(7) Å along the *a* axis, of 19.844(7) × 9.940 (7) Å along the *b* axis, of 8.169(1) × 8.169(1) Å along the *c* axis [figure 1(c)]. The crystallographically unique Co^{II} exhibits octahedral geometry coordinated with two oxygens from two $\{VO_4\}$ tetrahedra (Co–O 2.031(3) Å) and four nitrogens from three btx (Co–N 2.158 (4) and 2.168(5) Å). The btx can assume different conformations and consequently different N···N distances; the present N···N distance is 10.801 Å. As such, each cobalt is surrounded by four btx and two $[V_4O_{12}]^{4-}$, defining a six-connected node. If we only linked each $[Co_2O_4N_6]$ octahedron through btx with distance of 14.511 Å between each node, a 3-D cationic MOF $\{Co(btx)_2\}^{2+}$ is formed, as shown in figure 2. In summary, the overall net combining the inorganic and MOF composites is a 3-D binodal 4,6-connected self-catenated net with the $[V_4O_{12}]^{4-}$ cluster as 4-c node and Co1 as 6-c nodes $\{4^2{\cdot}5^5{\cdot}6^4{\cdot}7^2{\cdot}8^2\}_{Co1}\{5^6\}_{V4O12}$ (see figure 3). However, in spite of the complexity of the whole framework, **1** still possesses free void space in the [0 0 1] direction estimated to be about 1417.4 Å, which is 20.1% of the crystal volume.

Low nuclearity cyclic tetramer $[V_4O_{12}]^{4-}$ based-entangled structures are rare. Xu *et al*. reported an eight-connected self-catenated compound, $[Cu_4(bpp)_4V_4O_{12}]{\cdot}3H_2O$ (bpp = 1,3-bis(4-pyridyl)propane), in which the node is an isolated heterometallic cluster constructed from four copper (I) and $\{V_4O_{12}\}^{4-}$ [29]. Our group reported a new hybrid $[Co_2(biim)_3V_4O_{12}]{\cdot}4H_2O$ (biim = 1,1′-(butane-1,4-diyl)bis(imidazole)), which is a rare case of a self-catenated "ilc" network that displays an unusual $4^{24}{\cdot}5{\cdot}6^3$ topology [30]. Using the different organic ligand 1,4-bis(triazol-1-ylmethyl)benzene, **1** was obtained. Compound **1** can be viewed as a transition metal coordination complex-decorated POM. The role of organodiamine-liganted heterometals in organic–inorganic hybrids has been reviewed by Zubieta *et al*. [31]. However, compared with all the known structures of coordination complex decorated POMs, the structure of **1** is different. The SMC group $\{Co(btx)_2\}^{2+}$ in **1** forms a 3-D covalent framework, functioning as bridging groups to link POMs and templates to assist the formation of the 3-D inorganic framework. If the 3-D framework remains and keeps pores, voids or tunnels when the organic ligands are moved, the role of the 3-D SMC is obviously important and the overall synthesis strategy can be viewed as a top-down method.

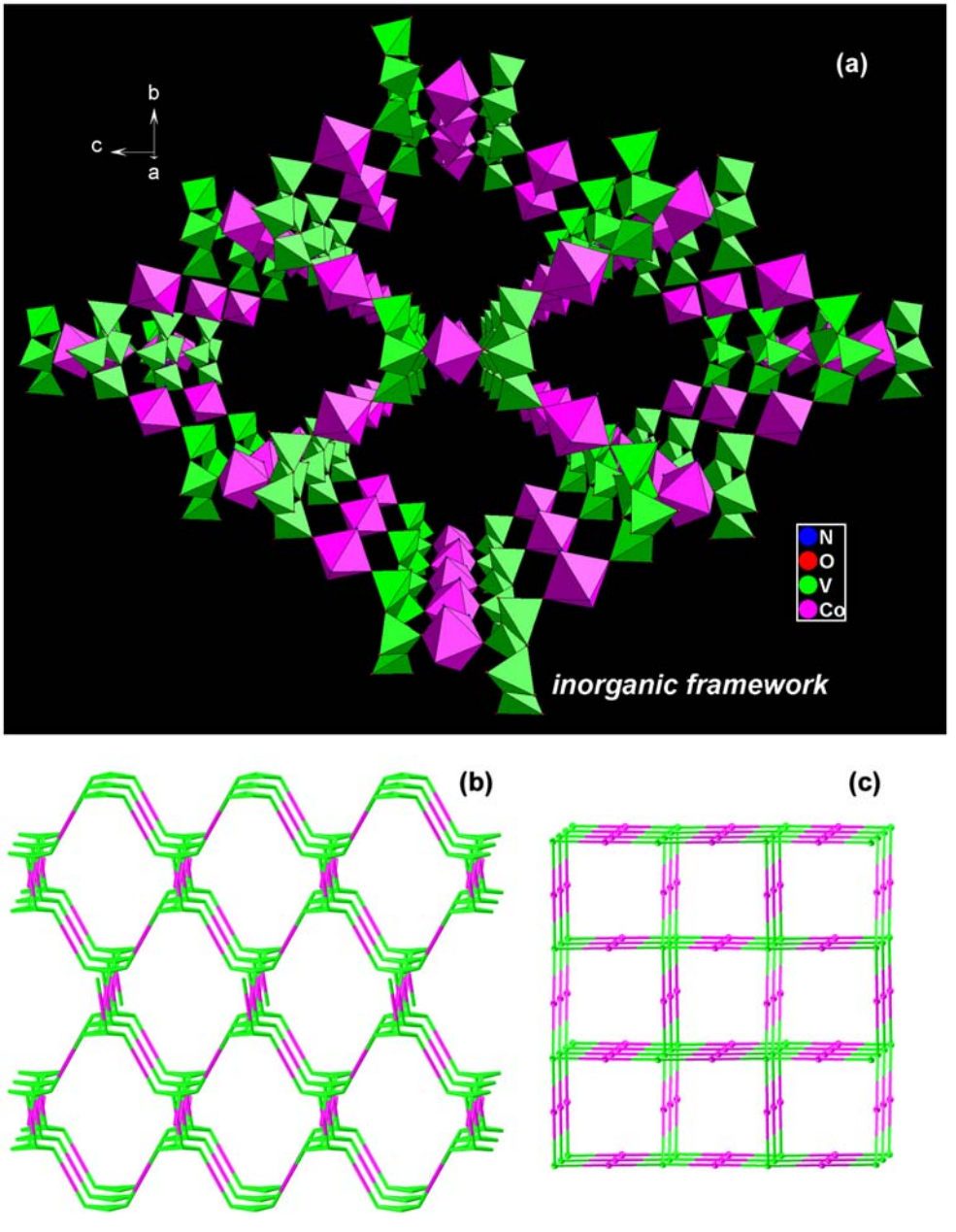

Figure 1. (a) Polyhedral and (b) schematic of the 3-D neutral inorganic framework constructed from $[V_4O_{12}]^{4-}$ and $\{CoN_4O_2\}^{2+}$ in **1**. (c) A simplified view of the inorganic framework with α-Po topology. The $\{V_4O_{12}\}^{4-}$ and $[CoN_4O_2]^{2+}$ were simplified to the green ball and purple ball, respectively. (see http://dx.doi.org/10.1080/00206814.2013.777835 for color version).

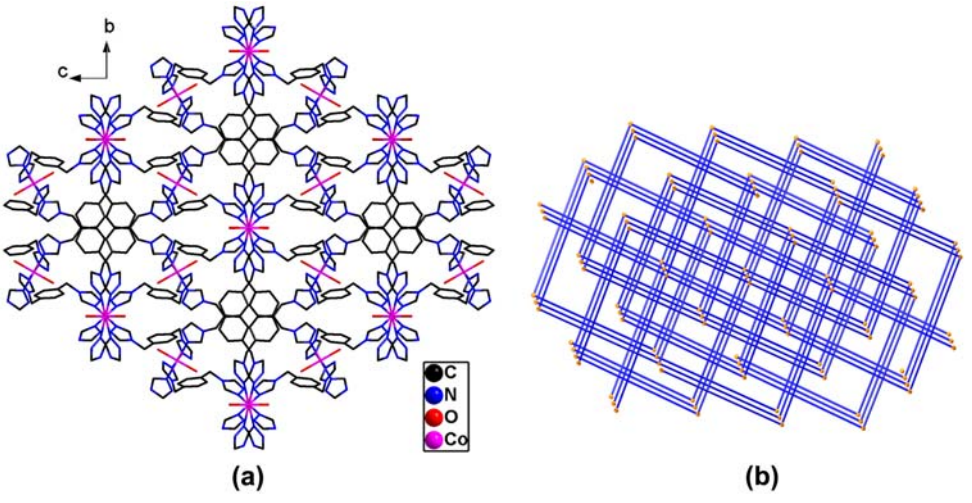

Figure 2. (a) Perspective and (b) topological representation of the 3-D MOF structure of $\{Co(btx)_2\}^{2+}$ in **1**.

3.2. *FT-IR Spectrum*

In the IR spectrum of **1** (figure S1), vibration modes for ν(V=O), ν(V–O–M) (M=V, or Co**1**) are observed at 954, 908, 811, 730, 642, 513, 465 cm^{-1}. The characteristic absorptions of organic ligands occur at 3115, 1521, 1423, 1351, 1285, 1198, 1133, 1012 cm^{-1}.

3.3. *Thermogravimetric and XRPD analyzes*

Thermogravimetric analysis was carried out in flowing N_2 with a heating rate of 10 °C min^{-1} from 25 to 600 °C for **1**, as shown in figure S2. The TG curve of **1** exhibits three major mass losses from 23 to 483 °C. The first weight loss of 2.64% at 25–72 °C is due to the loss of water, which may be coming from the crystal surface. The last two continuous weight losses of 64.22% at 300–486 °C are caused by decomposition of btx ligands. The whole weight loss of 66.84% is a little higher than calculated 65.28%. The simulated and experimental X-ray powder diffraction (XRPD) patterns of **1** are shown in figure 4(a) and (b). Their peak positions are in agreement with each other, indicating the phase purity of the products. The differences in intensity may be due to the preferred orientation of the powder samples. To check the stability of the networks, the as-synthesized crystalline **1** was heated in flowing N_2 with a heating rate of 5 °C min^{-1} and kept at 500 °C for 3 h to remove the organic ligands with a 43.12% weight loss to get the evacuated solid **1′**. The solid **1′** keeps the diamond-shaped appearance but its color changed from orange to brown. In the XRPD pattern of the evacuated crystalline solid **1′**, the main diffraction peaks before 20° disappear and some shift remarkably to higher 2θ values compared with those of as-synthesized **1** [figure 4(c)]. This may be due to severe deformation, or even destruction of the framework. The diffraction peaks are still sharp and indicate that the solid **1′** still remains in some properties of a crystalloid.

3.4. *Electrochemistry*

To determine the redox properties of **1**, a compound-bulk-modified CPE was fabricated as the working electrode due to their insolubility in most solvents [25]. Bulk-modified CPE is

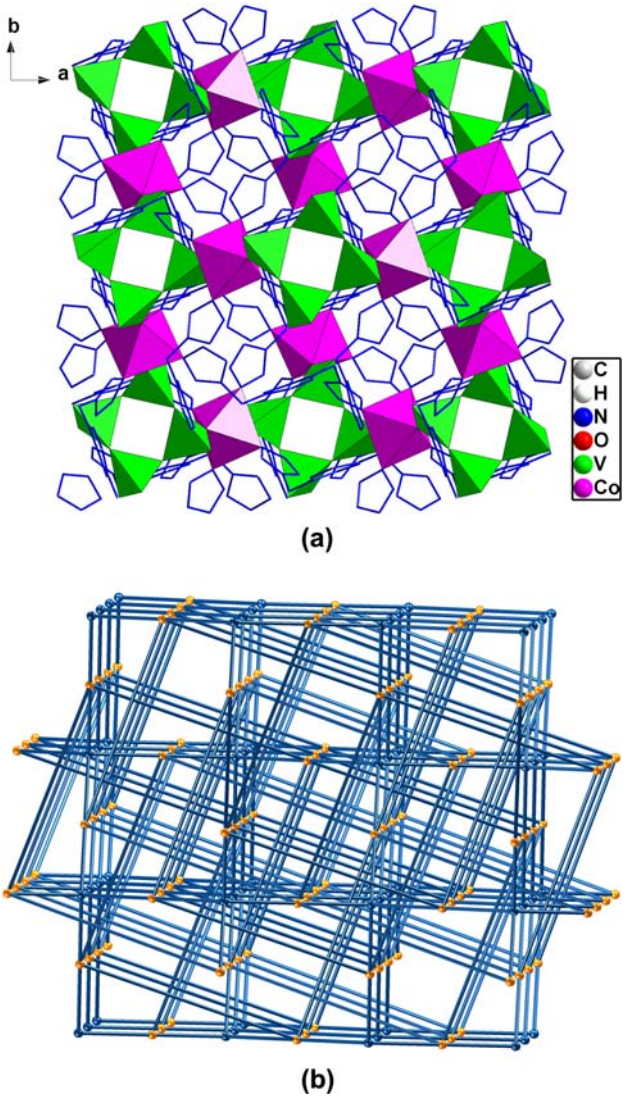

Figure 3. (a) Perspective and (b) ball-stick and polyhedral representation of the 2-D network of **1**. Schematic representation of the (4,6)-connected self-penetrating framework with $(5^6)(4^4{\cdot}5^9{\cdot}6^2)$ topology (blue and orange spheres represent the four- and six-connected nodes, respectively). (see http://dx.doi.org/10.1080/00206814.2013.777835 for color version).

a mixture of a modifier, graphite powder and pasting liquid, which has been widely applied in electrochemistry owing to its advantages of inexpensive, easy to handle and prepare. The bare graphite electrode did not show redox. Therefore, the peaks found in the figures reflect the properties of the compounds.

Figure 5(a) shows the voltammetric behavior of the working electrodes at 10 mV s^{-1} scan rate for **1** in 1 M H_2SO_4 aqueous solution. Compound **1** exhibits redox peaks I–I′ corresponding to V(V)/V(IV) one-electron processes. The mean peak potential $E_{1/2} = (E_{pa} + E_{pc})/2$ of the quasi-reversible redox peaks I–I′ is 0.784 V in **1**. The peak-to-peak separations between the corresponding anodic and cathodic peaks (ΔEp) at the working

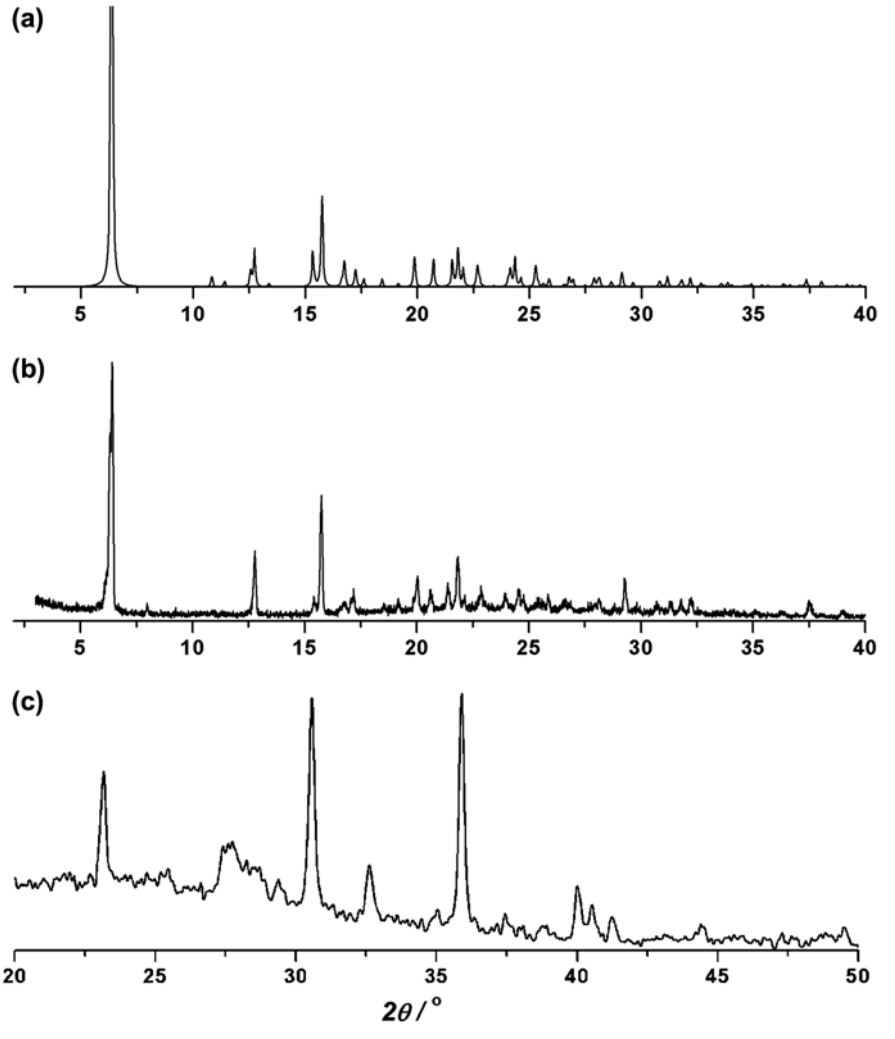

Figure 4. XRPD patterns of the (a) simulated, (b) experimental of **1,** and (c) evacuated crystalline solid **1′**.

electrode are larger than the reversible surface redox process, perhaps due to nonideal behavior. In figure 5(a), we assign the peaks II–II′ to Co(III)/Co(II) process for **1** [32, 33]. Figure 5(b) shows the cyclic voltammograms at different scan rates of **1**-CPE in 1 M H_2SO_4 aqueous solution. When the scan rate was changed from low to high, the peak potentials in **1** changed gradually with cathodic peak potentials shifted negative and the corresponding anodic peak potentials shifted positive. Peak-to-peak separation between the corresponding cathodic and anodic peaks in **1**-CEP increases with scan rate.

4. Conclusion

The 4,6-connected self-catenated net $Co_2(btx)_4V_4O_{12}$ was obtained, representing a 3-D organic–inorganic hybrid constructed from two different 3-D networks. The secondary metal complex plays a very important role in formation of **1**, both as the linker and as the template.

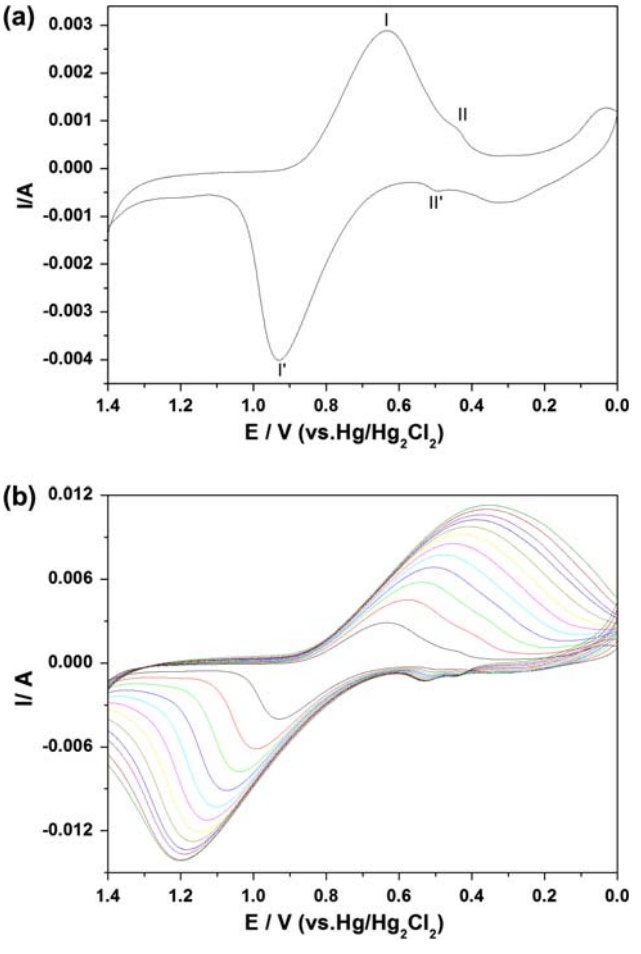

Figure 5. (a) The cyclic voltammogram in 1 M H_2SO_4 at 10 mV s^{-1} scan rate for **1**. (b) The cyclic voltammogram of **1** in 1 M H_2SO_4 at different scan rates (from inner to outer: 10–120 mV s^{-1}).

However, it is still impossible to control the synthesis of this kind of compounds. Studies are under way to reveal the synthetic rules and to explore their attractive properties.

Acknowledgments

This study was financially supported by National Science Foundation of China (81072337), China Postdoctoral Science Foundation (20100481064 and 2012T50307) and S& Development Project Foundation of Jilin Province (201101057), General Administration of Quality Supervision, Inspection and Quarantine of China Project (2009IK151).

References

[1] J.L.C. Rowsell, O.M. Yaghi. *J. Am. Chem. Soc.*, **128**, 1304 (2006).
[2] Catenanes, Rotaxanes, Knots, *A Journey Through the World of Molecular Topology*, J.P. Sauvage, C. Dietrich-Buchecker (Eds.), Wiley–VCH, Weinheim (1999).

[3] L. Carlucci, G. Ciani, D.M. Proserpio. *Networks, Topologies, and Entanglements in Making Crystals by Design – Methods, Techniques and Applications*, D. Braga, G. Grepioni (Eds.), Wiley–VCH, Weinheim (2007), Ch. 1.3.
[4] X.H. Bu, M.L. Tong, H.C. Chang, S. Kitagawa, S.R. Batten. *Angew. Chem. Int. Ed.*, **43**, 192 (2004).
[5] S.R. Batten, R. Robson. *Angew. Chem. Int. Ed.*, **37**, 1460 (1998).
[6] L. Carlucci, G. Ciani, D.M. Proserpio. *Coord. Chem. Rev.*, **246**, 247 (2003).
[7] X.L. Wng, C. Qin, E.B. Wang, Z.M. Su, Y.G. Li, L. Angew. *Chem. Int. Ed.*, **45**, 904 (2006).
[8] C. Qin, X.L. Wang, E.B. Wang, Z.M. Su. *Inorg. Chem.*, **47**, 5555 (2008).
[9] H. Wu, J. Yang, Y.Y. Liu, J.F. Ma. *Cryst. Growth Des.*, **12**, 2272 (2012).
[10] J. Yang, J.F. Ma, S.R. Batten. *Chem. Commun.*, **48**, 7899 (2012).
[11] Z.M. Zhang, J. Liu, Y.G. Li, S. Yao, E.B. Wang, X.L. Wang. *J. Solid State Chem.*, **183**, 228 (2010).
[12] M.T. Pope. *Heteropoly and Isopoly Oxometalates*, Springer, Berlin (1983).
[13] C.L. Hill. *Chem. Rev.*, **98**, 327 (1998).
[14] C.D. Wu, C.Z. Lu, H.H. Zhuang, J.S. Huang. *J. Am. Chem. Soc.*, **124**, 3836 (2002).
[15] I.S. Tidmarsh, R.H. Laye, P.R. Brearley, M. Shanmugam, E.C. Sañdo, L. Sorace, A. Caneschib, E.J.L. McInnes. *Chem. Commun.*, **2560**, (2006).
[16] L. Chen, F.L. Jiang, Z.Z. Lin, Y.F. Zhou, C.Y. Yue, M.C. Hong. *J. Am. Chem. Soc.*, **127**, 8588 (2005).
[17] C.R. Walk. In *Lithium Batteries*, J.P. Gabano (Ed.), Academic Press, New York (1983).
[18] D.C. Crans, J.J. Smee, E. Gaidamauskas, L. Yang. *Chem. Rev.*, **104**, 849 (2004).
[19] M.I. Khan, E. Yohannesa, R.J. Doedens. *Angew. Chem., Int. Ed.*, **38**, 1292 (1999).
[20] Y.F. Qi, E.B. Wang, J. Li, Y.G. Li. *J. Solid State Chem.*, **182**, 2640 (2009).
[21] Y.F. Qi, C.P. Lv, Y.G. Li, E.B. Wang, J. Li, X.L. Song. *Inorg. Chem. Commun.*, **13**, 384 (2010).
[22] Y.P. Xie, T.C. Mak. *Chem. Commun.*, **48**, 1123 (2012).
[23] A. Tripathi, T. Hughbanks, A. Clearfield. *J. Am. Chem. Soc.*, **125**, 10528 (2003).
[24] L. Carlucci, G. Ciani, D.M. Proserpio, S. Rizzato. *Chem. Eur. J.*, **8**, 1519 (2002).
[25] X.L. Wang, C. Qin, E.B. Wang, Z.M. Su, Y.G. Li, L. Angew. *Chem. Int. Ed.*, **45**, 7411 (2006).
[26] X.L. Wang, Z.H. Kang, E.B. Wang, C. Mater. *Lett.*, **56**, 393 (2002).
[27] G.M. Sheldrick. *SHELXS-97*, *Program for Crystal Structure Solution*, University of Göttingen, Germany (1997).
[28] G.M. Sheldrick. *SHELXL-97*, *Program for Crystal Structure Refinement*, University of Göttingen, Germany (1997).
[29] O. Delgado-Friedrichs, M. O'Keeffe, O.M. Yaghi. *Acta Crystallogr.*, *Sect. A*, **A59**, 15 (2003).
[30] Y.F. Qi, D.R. Xiao, E.B. Wang, Z.M. Zhang, X.L. Wang. *Aust. J. Chem.*, **60**, 871 (2007).
[31] D.J. Chesnut, D. Hagrman, P.J. Zapf, R.P. Hammond, R. LaDuca, R.C. Haushalter, J. Zubieta. *Coord. Chem. Rev.*, **190–192**, 737 (1999).
[32] B.S. Bassil, U. Kortz, A.S. Tigan, J.M.C. Juan, B. Keita, P. de Oliveira, L. Nadjo. *Inorg. Chem.*, **44**, 9360 (2005).
[33] L. Lisnard, P. Mialane, A. Dolbecq, J. Marrot, J.M.C. Juan, E. Coronado, B. Keita, P.D. Oliveira, L. Nadjo, F. Sécheresse. *Chem. Eur. J.*, **13**, 3525 (2007).